20. Islam, M. N., Rafiuddin, M. Ahmed, A. U. and Kolli, R. K., Calibration of PRECIS in employing future scenarios in Bangladesh. *Int. J. Climatol*., 2008, **28**, 617–628.
21. Xu, Y., Jones, R., Lin, E. and Lin, W., Analysis on the climate change responses over China under SRES B_2 scenario using PRECIS. *Chin. Sci. Bull*., 2006, **51**, 2260–2267.
22. Slafer, G. A. and Rawson, H. M., Base and optimum temperatures vary with genotype and stage of development in wheat. *Plant Cell Environ*., 1995, **18**, 671–679.
23. De Costa, W. A. J. M., Weerakoon, W. M. W., Herath, H. M. L. K., Amaratunga, K. S. P. and Abeywardena, R. M. I., Physiology of yield determination of rice under elevated carbon dioxide at high temperatures in a subhumid tropical climate. *Field Crops Res*., 2006, **96**(2–3), 336–347.
24. Fletcher, A. L. and Jamieson, P. D., Causes of variation in the rate of increase of wheat harvest index. *Field Crops Res*., 2009, **113**(3), 268–273.
25. Challinor, A. J., Wheeler, T. R., Craufurd, P. Q., Ferro, C. A. T. and Stephenson, D. B., Adaptation of crops to climate change through genotypic responses to mean and extreme temperatures. *Agric. Ecosyst. Environ*., 2007, **119**, 190–204.
26. Whaley, E., Kirby, J. M., Spink, J. H., Foulkes, M. J. and Sparkes, D. L., Frost damage to winter wheat in the UK: the effect of plant population density. *Eur. J. Agron.*, 2004, **21**(1), 105–115.
27. Lang, P., Zhang, C. K., Ebel, R. C., Dane, F. and Dozier, W. A., Identification of cold accelerated genes in leaves of citrus by mRNA differential display. *Gene*, 2005, **359**, 111–118.
28. Fuller, M. P., Fuller, A. M., Kaniouras, S., Christophers, J. and Fredericks, T., The freezing characteristics of wheat at ear emergence. *Eur. J. Agron*., 2007, **26**(4), 435–441.
29. Fowler, H. J., Ekström, M., Kilsby, C. G. and Jones, P. D., New estimates of future changes in extreme rainfall across the UK using regional climate model integrations. 1. Assessment of control climate. *J. Hydrol.*, 2005, **300**(1–4), 212–233.
30. Mailhot, A., Duchesne, S., Caya, D. and Talbot, D., Assessment of future change in intensity–duration–frequency (IDF) curves for Southern Quebec using the Canadian Regional Climate Model (CRCM). *J. Hydrol.*, 2007, **347**(1–2), 197–210.
31. Roosmalen, L. V., Christensen, J. H., Butts, M. B., Jensen, K. H. and Refsgaard, J. C., An intercomparison of regional climate model data for hydrological impact studies in Denmark. *J. Hydrol.*, 2010, **380**(3–4), 406–419.
32. Blenkinsop, S. and Fowler, H. J., Changes in drought frequency, severity and duration for the British Isles projected by the PRUDENCE regional climate models. *J. Hydrol*., 2007, **342**(1–2), 50–71.

ACKNOWLEDGEMENTS. We thank the Indian Institute of Tropical Meteorology, Pune for providing the PRECIS outputs for this study, through NATCOM, Ministry of Environment and Forests, Government of India.

Received 17 August 2013; revised accepted 3 November 2014

The influence of sugar–phosphate backbone on the stacking interaction in B-DNA helix formation

Sumit Mittal[1], Brijesh Kumar Mishra[2,3] and N. Sathyamurthy[1,2,*]

[1]Indian Institute of Science Education and Research Mohali, Manauli 140 306, India
[2]Department of Chemistry, Indian Institute of Technology Kanpur, Kanpur 208 016, India
[3]International Institute of Information Technology Bangalore, Bengaluru 560 100, India

The influence of sugar–phosphate backbone on the stacking interaction in the adenine…thymine base-pair dimer $(A…T)_2$ has been studied using the density functional theoretic method and the dispersion-corrected density functional BLYP-D3 and the triple-zeta quality basis set def2-TZVP. In the absence of the sugar–phosphate backbone, several stacked conformers were obtained with a small difference in their stabilization energy values (–20 to –25 kcal/mol). However, the presence of the sugar–phosphate backbone limits the movement of the two A…T units, and yet the stacking interaction remains significant (–19.4 kcal/mol). Despite the constraints imposed by the backbone, the dimer $(A…T)_2$ is found to retain its favourable geometry. The influence of sodium ions on the geometry and the interaction energy is found to be negligible.

Keywords: B-DNA helix formation, BLYP-D3, stacking interaction, sugar–phosphate backbone.

THE classic double-helical structure of B-DNA, proposed by Watson and Crick[1], is governed by hydrogen bonds between the Watson–Crick (WC) base pairs of anti-parallel strands, stacking interactions between nucleobases, and covalent bonds between the base pairs and the sugar–phosphate units[2–4]. The stabilization energy value associated with the stacking interaction between adenine, guanine, cytosine and thymine dimers ranges from 10 to 17 kcal/mol (ref. 3). In contrast, the strength of multiple hydrogen bonds between base pairs falls between 20 and 30 kcal/mol. Therefore, it can be concluded that the contribution of the stacking interaction to the overall stability of DNA is comparable to that of the hydrogen bonds. Although it is generally perceived that hydrogen bonding is primarily governed by electrostatic forces and π-stacking interaction by dispersion forces[4–7], in the recent past there have been instances where such perceptions have been challenged[8,9]. A recent molecular dynamics (MD) simulation study[10] showed that in the absence of the dispersion energy component, the double-helical structure is transformed into a straight ladder-like structure. The relative

*For correspondence. (e-mail: nsath@iitk.ac.in)

orientation of one base pair with respect to another can be described using six degrees of freedom, namely, twist, roll and tilt, which are rotational parameters, and slide, shift and rise, which are translational parameters[11].

Extensive quantum chemical calculations have been used to analyse the nature of the base-pair stacking using a wide range of methods and basis sets[12–16]. Hobza and Šponer[17] reported the stacking energy values for homodimers of cytosine, guanine and uracil using the second-order Møller–Plessett perturbation (MP2) theoretic method in the complete basis set (CBS) limit. Subsequently, the interaction energy values for a set of 10 stacked DNA base pairs representing the gas phase minimum structures with respect to the helical parameters (rise, twist and propeller twist) were reported at the estimated CCSD(T)/CBS limit[18]. Potential energy scans with respect to the twist parameter for each of the DNA base-pair steps were generated by Cooper *et al.*[19] using the van der Waals-density functional theory (vdW-DFT). This study reported the twist angle to be $34° \pm 10°$ for the energetic minimum structures, close to the average value of the twist angle for B-DNA ($36° \pm 7°$)[19].

A common feature of the computational studies available so far is the use of the truncated models. DNA nucleosides and nucleotides are typically modelled as nucleobases with the sugar–phosphate backbone replaced by hydrogen atoms or methyl groups. The use of such truncated systems enables the determination of the strength of the stacking interaction and also keeps the computations viable. As a result, the influence of the deoxyribose sugar–phosphate backbone, which imposes certain constraints over the stacked base pairs, has not been studied in detail. In principle, the backbone can be considered as a substituent on the nucleobases and substituents have been shown to alter the stacking interaction and structures significantly[20–25]. For example, the potential energy surface of benzene dimer possesses at least two energy minima, one corresponding to the *T*-shaped geometry and the other to the parallel-displaced geometry. However, it is to be emphasized that only the *T*-shaped geometry of the benzene dimer has been observed experimentally[26]. On the other hand, for the pyridine dimer, antiparallel-stacked geometry was found to be the most stable[27]. Also for the toluene dimer, the stacked configuration was found to be preferred over the *T*-shaped geometry, in gas phase as well as in aqueous medium[28]. Therefore, it can be deduced that the presence of heteroatoms/substitutents favours a stacked geometry.

The conformation of the sugar moiety is considered a dominant factor in the determination of the type of the DNA helix (A, B or Z)[29]. The MP2 theory-based computations performed by Churchill *et al.*[30] revealed that the presence of sugar–phosphate backbone has a significant influence over the strength of the stacking interaction. Further analysis showed that there is a direct interaction between the backbone and the base pairs, which enhances the stability of the overall complex[31]. In a more recent work, the passive role of the backbone in guiding the helical shape of DNA was predicted by Sherrill and coworkers using the symmetry-adapted perturbation theory (SAPT) computations[32]. The helical parameters rise and twist, corresponding to the minimum energy geometry of the stacked base pairs were found to be in good agreement with the corresponding values in the crystal structure of B-DNA.

There are a few studies available in the literature addressing the influence of sugar–phosphate backbone on the structure and stability of the DNA helix[33–35]. However, a systematic theoretical investigation of the base-pair dimers with/without sugar–phosphate backbone would quantify the role of the backbone in governing the helical shape of B-DNA.

Here, we have undertaken a detailed DFT study of the role of the sugar–phosphate backbone on non-covalent interactions present in B-DNA and its importance in the double-helix formation. Stacking interaction energy values for the base-pair dimers with and without the backbone are computed. The six geometry parameters (twist, roll, tilt, slide, shift and rise) are estimated. The role of Na^+ ions in the structure and energetics is also studied.

An accurate estimation of non-covalent interactions is a challenging task[36,37]. Density functionals like B3LYP and PBE seem to be reliable in describing hydrogen bonds, but they fail to describe the dispersion interaction, which is a dominant force in the stacking interaction of aromatic systems. Some of the recently developed functionals like the dispersion-corrected density functionals DFT-D[38], B2PLYP[39] and the M05/M06 series[40], have shown remarkable success in accurately accounting for the dispersion interaction. The DFT-D functionals were constructed by adding an empirical dispersion-correction term to the traditional DFT methods[41]. Revised dispersion-correction terms (DFT-D3 methods) were recently introduced and reported to yield accurate energies, and a number of new functionals like BLYP-D3, B3LYP-D3, and PBE-D3 are now available[42–44]. Grimme and coworkers[45] assessed the efficacy of various DFT functionals in accounting for the non-covalent interaction in three databases (S22, S66 and S66x8) and found that BLYP-D3 performed exceedingly well over all intermolecular distances, particularly in the long range.

In the present work, the influence of the sugar–phosphate backbone on the stacking interaction present in B-DNA was studied by computing the stacking interaction energy values and the base-step parameters for the adenine…thymine base-pair dimer $(A…T)_2$. Reference geometries of these base-pair dimers were obtained from high-resolution X-ray crystallographic data of the oligonucleotide with nucleoside database (NDB) ID: BD0005 (ref. 46). It is known that a small error in the experimental inter-base distance can cause a major bias in the energy calculation, leading to a false interpretation of the

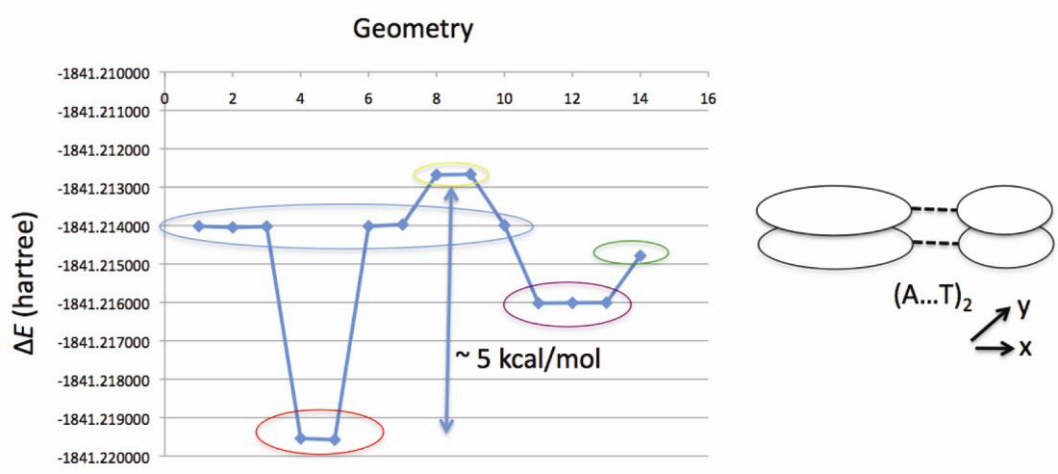

Figure 1. Total energy values for the fully optimized $(A\ldots T)_2$ geometries obtained using the DFT method and the BLYP-D3 functional and the def2-SVP basis set.

results. Therefore, the geometry of the base-pair dimer with and without the sugar–phosphate backbone was fully optimized using the BLYP-D3 functional and def2-SVP and def2-TZVP basis sets. It is to be mentioned that the resolution of the identity (RI) approximation was used to speed up the calculations[47]. All the electronic structure calculations were carried out using the TURBOMOLE suite of programs[48]. To determine the stacking interaction energy, the sugar–phosphate backbone atoms were removed. Single-point energy calculation was carried out using the BLYP-D3/def2-TZVP method and the total stacking interaction energy value (ΔE_{int}) was obtained by computing the interaction energy for the complex and the base pairs as

$$\Delta E_{\text{int}} = \Delta E\,[(A\ldots T)_2] - 2\,[\Delta E\,(A\ldots T)], \qquad (1)$$

where A and T denote the bases adenine and thymine respectively. The six base-step parameters for all the geometries were determined using the web-based interface of 3DNA suite of programs, W3DNA[49]. Electron density and bond critical points for the stacked pairs were obtained by performing atoms-in-molecules (AIM) calculations using the AIM-2000 package[50].

Several input geometries for the dimer of the adenine…thymine base pair $(A\ldots T)_2$, were constructed manually by shifting one base pair with respect to the other in horizontal (x) and lateral (y) directions, as shown in Figure 1. Full geometry optimization calculations were carried out using the functional BLYP-D3 and the basis set def2-SVP to explore the potential energy surface and the local minima and the results obtained are depicted in Figure 1. At least five local minima were observed, with the largest energy difference between two minima being 5 kcal/mol. Subsequently, for quantitative prediction the most stable geometry was re-optimized using the triple-zeta quality basis set (def2-TZVP) and the resultant geometry is shown in Figure 2. It can be seen from the figure that in the most stable geometry of $(A\ldots T)_2$ the individual base pairs form a bowl-shaped geometry and the orientation of one base pair is almost perpendicular with respect to the other. The stabilization energy for this most stable stacked dimer is computed to be –24.85 kcal/mol, which is comparable to the hydrogen bond energy between bases A and T. Therefore, it can be safely assumed that stacking interactions are as important as hydrogen bonds in stabilizing large helical structures of DNA.

To study the influence of the sugar–phosphate backbone on the structure and stability of $(A\ldots T)_2$, the dimer geometry was obtained from the high resolution X-ray crystallographic data of an oligonucleotide (NDB code: BD0005). The coordinates obtained from the X-ray data were fully optimized using the BLYP-D3/def2-TZVP method and the resulting geometry is reproduced in Figure 3. This structure contains four sugar moieties and two phosphate units. It is obvious that the mutual orientation of the two A…T base pairs in the presence of the backbone is significantly different from that in free $(A\ldots T)_2$. Clearly, the presence of the sugar–phosphate backbone imposes a constraint and hence the shift and rotation of the two base pairs are limited. It is to be noted that each of the phosphate units has a negative charge on the oxygen atom. Thus, the whole structure carries a total of two negative charges.

To obtain the stacking interaction in the presence of the backbone, sugar–phosphate atoms were removed from this structure (Figure 4 *a*). The stacking interaction of the truncated geometry was calculated to be –19.39 kcal/mol at the BLYP-D3/def2-TZVP level. This is ~5 kcal/mol less stable than the most stable free $(A...T)_2$. Therefore, it can be deduced that due to the constraints imposed by the sugar–phosphate backbone, $(A\ldots T)_2$ loses ~5 kcal/mol stability. Interestingly, full optimization of the truncated geometry (Figure 4 *a*) quickly led to a converged local

minimum, as shown in Figure 4 *b*. The interaction energy for the optimized geometry was found to be –20.12 kcal/mol at the BLYP-D3/def2-TZVP level. This is slightly more stable (by 0.73 kcal/mol) than the constrained geometry (Figure 4 *a*). Also, the two geometries do not differ much in terms of their base step parameters (twist, rise, slide, etc.), as shown in Table 1. Therefore, despite the sugar–phosphate constraint, the stacking interaction between two base pairs remains significantly large and the geometrical parameter values with the backbone are found to be close to those without the backbone.

We have studied the role of the sodium ions (Na^+) on the structure and energetics of $(A\ldots T)_2$ with the backbone. For this purpose, two sodium ions were placed close to the phosphate units, as they contain the negative charge. The fully optimized geometry of $(A\ldots T)_2$ in the presence of the backbone and the two Na^+ ions at the BLYP-D3/def2-TZVP level is depicted in Figure 5. It can be seen that each of the sodium ions interacts with two oxygen atoms. The influence of Na^+ on the overall structure was found to be minimal. The stacking interaction of the truncated structure (in the absence of Na^+ and the backbone) was computed to be –19.57 kcal/mol, which is close to the interaction energy value when Na^+ ions are present.

The negligible influence of Na^+ ions on the stacking interaction of $(A\ldots T)_2$ can be explained using the electron density and a bond critical point analysis. Parthasarathi *et al.*[51] have pointed out the correlation between the electron density at the bond critical points and the strength of hydrogen bond and van der Waals interactions. We have performed an AIM analysis and the data obtained in terms of the electron density (ρ) and the Laplacian of the electron density ($=^2\rho$) are summarized in the Supporting Information (see online) along with corresponding figures. The results indicate that there is no significant change in the electron density at the (3, –1) bond critical points between the stacked base pairs when the Na^+ ions and sugar–phosphate backbone are added. This is

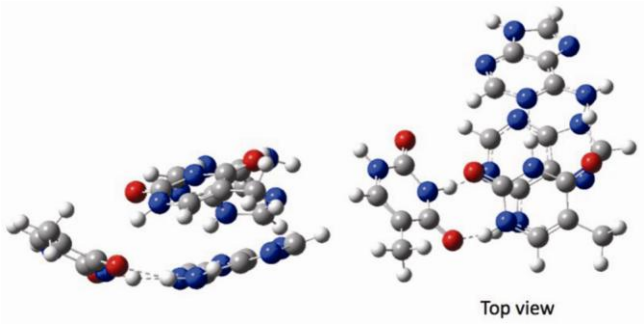

Figure 2. Fully optimized geometry of $(A\ldots T)_2$ obtained using the DFT method and the BLYP-D3 functional and the def2-TZVP basis set. Colour code: Grey for carbon, blue for nitrogen, red for oxygen and white for hydrogen atoms.

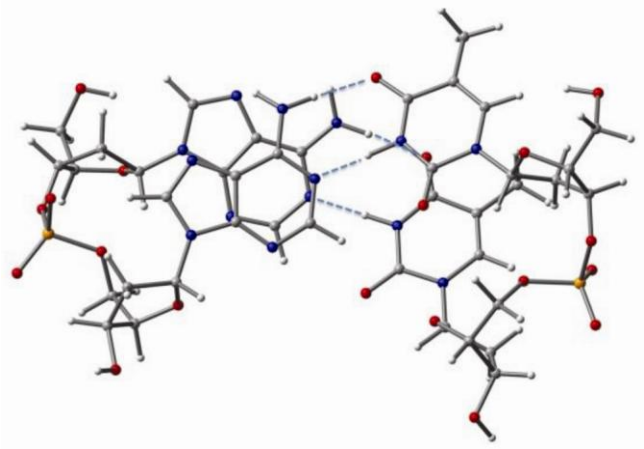

Figure 3. Optimized geometry of $(A\ldots T)_2$ in the presence of the sugar–phosphate backbone obtained using the DFT method and the BLYP-D3 functional and the def2-TZVP basis set. Colour code: Grey for carbon, blue for nitrogen, red for oxygen, white for hydrogen atoms and yellow for phosphorus atoms.

Table 1. Base-pair step parameters for $(A\ldots T)_2$ with and without considering the sugar–phosphate backbone

Motion	Figure 4 *a*	Figure 4 *b*	With Na^+	Input (BD0005)
Shift	0.03	0.02	0.0	0.1
Slide	–0.14	–0.13	0.01	–0.3
Rise	3.21	3.25	3.17	3.3
Twist	43.99	43.63	40.74	38.82
Roll	5.38	5.11	0.77	–1.94
Tilt	–3.54	–3.01	–4.00	–0.69

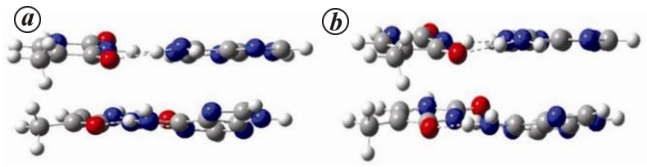

Figure 4. $(A\ldots T)_2$ geometry optimized at the DFT/BLYP-D3/def2-TZVP level of theory in the presence (***a***) and absence (***b***) of the sugar–phosphate backbone. Colour code: Same as in Figure 2.

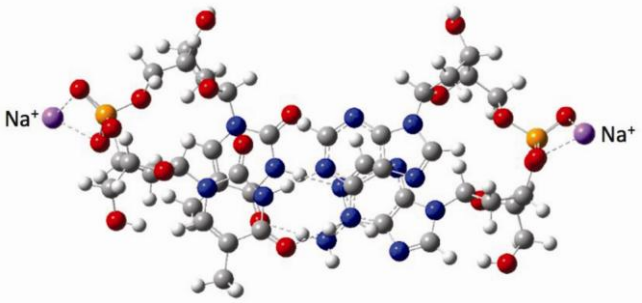

Figure 5. Optimized geometry of $(A\ldots T)_2$ at the DFT/BLYP-D3/def2-TZVP level of theory in the presence of sugar–phosphate backbone and two Na^+ ions. Colour code: Same as in Figure 2.

understandable due to the large distance (~9.0 Å) between the Na^+ ions and the π-centre of the nucleobases.

The base-pair step parameters for $(A\ldots T)_2$ with and without the backbone and in the presence of Na^+ ions are listed in Table 1. All six parameters for the dimer with and without the backbone are found to be similar. But, they differ significantly from those of the initial geometry obtained from the nucleoside database (NDB ID: BD0005). The difference in the geometry parameters can be accounted for by the difference in force-field parameters used during crystal structure refinement.

Based on our calculations of the geometry and energy of the $(A\ldots T)_2$ unit with and without the backbone, it is inferred that, despite the constraints imposed by the backbone, the $(A\ldots T)_2$ dimer retains its near-optimal geometry and the stacking interaction contributes significantly (~ –20 kcal/mol per stacked unit) to the overall stabilization of the DNA structure. The stacking interaction between bases is comparable to the hydrogen bond energy between them, which is assumed to play a primary role in stabilizing large DNA helical structures. In the absence of the backbone several conformers of the dimer corresponding to various local minima were obtained, with the most stable geometry having a stacking interaction of ~ –25 kcal/mol. The influence of sodium ions on both the energy and the geometrical parameters was found to be negligible. A study of larger oligomers (trimer, tetramer and pentamer) and the influence of solvents on the geometry is in progress.

1. Watson, J. D. and Crick, F. H. C., Molecular structure of nucleic acids. *Nature*, 1953, **171**, 737–738.
2. Hobza, P. and Müller-Dethlefs, K., *Non-Covalent Interactions: Theory and Experiment*, RSC Publishing, London, 2009.
3. Hobza, P. and Šponer, J., Structure, energetics and dynamics of the nucleic acid base pairs: nonempirical *ab initio* calculations. *Chem. Rev.*, 1999, **99**, 3247–3276.
4. Hobza, P., Šponer, J. and Polášek, M., H-bonded and stacked DNA base pairs: cytosine dimer. An *ab initio* second order Møller–Plesset perturbation theory. *J. Am. Chem. Soc.*, 1995, **117**, 792–798.
5. Jurečka, P., Šponer, J., Černy, J. and Hobza, P., Benchmark database of accurate (MP2 and CCSD(T) complete basis set limit) interaction energies of small model complexes, DNA base pairs, and amino acid pairs. *Phys. Chem. Chem. Phys.*, 2006, **8**, 1985.
6. Hesselmann, A., Jansen, G. and Schütz, M., Interaction energy contributions of H-bonded and stacked structures of the AT and GC DNA base pairs from the combined density functional theory and intermolecular perturbation theory approach. *J. Am. Chem. Soc.*, 2006, **128**, 11730–11731.
7. Pérez-Casas, S., Hernández-Trujillo, J. and Costas, M., Experimental and theoretical study of aromatic–aromatic interactions. Association enthalpies and central and distributed multipole electric moments analysis. *J. Phys. Chem. B*, 2003, **107**, 4167–4174.
8. Williams, C. W., Zare, R. N. and Arunan, E., Do identical polar diatomic molecules form stacked or linear dimers? *Resonance*, 2014, **19**, 704–712.
9. Weinhold, F. and Klein, R. A., Anti-electrostatic hydrogen bonds. *Angew. Chem.*, 2014, **126**, 11396–11399.
10. Černy, J., Kabeláč, P. and Hobza, P., Double-helical → ladder structural transition in the B-DNA is induced by a loss of dispersion energy. *J. Am. Chem. Soc.*, 2008, **130**, 16055–16059.
11. Hunter, C. A. and Lu, X.-J., DNA base-stacking interactions: a comparison of theoretical calculations with oligonucleotide X-ray crystal structures. *J. Mol. Biol.*, 1997, **265**, 603–619.
12. Antony, J. and Grimme, S., Density functional theory including dispersion corrections for intermolecular interactions in a large benchmark set of biologically relevant molecules. *Phys. Chem. Chem. Phys.*, 2006, **8**, 5287–5293.
13. Hill, G., Forde, G., Hill, N., Lester Jr, W. A., Sokalski, W. A. and Leszczynski, J., Interaction energies in stacked DNA bases? How important are electrostatics? *Chem. Phys. Lett.*, 2003, **381**, 729–732.
14. Price, S. L. and Stone, A. J., The electrostatic interactions in van der Waals complexes involving aromatic molecules. *J. Chem. Phys.*, 1987, **86**, 2859.
15. Jurečka, P., Šponer, J. and Hobza, P., Potential energy surface of the cytosine dimer: MP2 complete basis set limit interaction energies, CCSD(T) correction term, and comparison with the AMBER force field. *J. Phys. Chem. B*, 2004, **108**, 5466–5471.
16. Šponer, J. and Hobza, P., Nonplanar geometries of DNA bases. *Ab initio* second order Møller–Plesset study. *J. Phys. Chem.*, 1994, **98**, 3161–3164.
17. Hobza, P. and Šponer, J., Toward true DNA base-stacking energies: MP2, CCSD(T) and complete basis set calculations. *J. Am. Chem. Soc.*, 2002, **124**, 11802–11808.
18. Šponer, J., Jurečka, P., Marchan, I., Luque, F. J., Orozco, M. and Hobza, P., Nature of base stacking: reference quantum-mechanical stacking energies in ten unique B-DNA base-pair steps. *Chem. Eur. J.*, 2006, **12**, 2854–2865.
19. Cooper, V. R., Thonhauser, T., Puzder, A., Schröder, E., Lundqvist, B. I. and Langreth, D. C., Stacking interactions and the twist of DNA. *J. Am. Chem. Soc.*, 2008, **130**, 1304–1308.
20. Raju, R. K., Bloom, J. W. G., An, Y. and Wheeler, S. E., Substituent effects on non-covalent interactions with aromatic rings: insights from computational chemistry. *Chem. Phys. Chem.*, 2011, **12**, 3116–3130.
21. Hohenstein, E. G., Duan, J. and Sherrill, C. D., Origin of the surprising enhancement of electrostatic energies by electron-donating substituents in substituted sandwich benzene dimers. *J. Am. Chem. Soc.*, 2011, **133**, 13244–13247.
22. Sinnokrot, M. O. and Sherrill, C. D., Unexpected substituent effects in face-to-face π-stacking interactions. *J. Phys. Chem. A*, 2003, **107**, 8377–8379.
23. Lee, E. C., Kim, D., Jurečka, P., Tarakeshwar, P., Hobza, P. and Kim, K. S., Understanding of assembly phenomena by aromatic-aromatic interactions: benzene dimer and the substituted systems. *J. Phys. Chem. A*, 2007, **111**, 3446–3457.
24. Clements, A. and Lewis, M., Arene–cation interactions of positive quadrupole moment aromatics and arene–anion interactions of negative quadrupole moment aromatics. *J. Phys. Chem. A*, 2006, **110**, 12705–12710.
25. Wheeler, S. E., Local nature of substituent effects in stacking interactions. *J. Am. Chem. Soc.*, 2011, **133**, 10262–10274.
26. Chandrasekaran, V., Biennier, L., Arunan, E., Talbi, D. and Georges, R., Direct infrared absorption spectroscopy of benzene dimer. *J. Phys. Chem. A*, 2011, **115**, 11263–11268.
27. Mishra, B. K. and Sathyamurthy, N., π–π interaction in pyridine. *J. Phys. Chem. A*, 2005, **109**, 6–8.
28. Chipot, C., Jaffe, R., Maigret, B., Pearlman, D. A. and Kollman, P. A., Benzene dimer: a good model for π–π interactions in proteins? A comparison between the benzene and the toluene dimers in the gas phase and in an aqueous solution. *J. Am. Chem. Soc.*, 1996, **118**, 11217–11224.
29. Matta, C. F., Castillo, N. and Boyd, R. J., Extended weak bonding interactions in DNA: π-stacking (base–base), base–backbone, and

backbone–backbone ineractions. *J. Phys. Chem. B*, 2006, **110**, 563–578.
30. Churchill, C. D. M., Navarro-Whyte, L., Rutledge, L. R. and Wetmore, S. D., Effects of the biological backbone on DNA–protein stacking interactions. *Phys. Chem. Chem. Phys.*, 2009, **11**, 10657–10670.
31. Churchill, C. D. M., Rutledge, L. R. and Wetmore, S. D., Effects of the biological backbone on stacking interactions at DNA-protein interfaces: the interplay between the backbone–π and π–π components. *Phys. Chem. Chem. Phys.*, 2010, **12**, 14515–14526.
32. Parker, T. M., Hohenstein, E. G., Parrish, R. M., Hud, N. V. and Sherrill, C. D., Quantum-mechanical analysis of the energetic contributions to π-stacking in nucleic acids versus rise, twist and slide. *J. Am. Chem. Soc.*, 2013, **135**, 1306–1316.
33. Wang, S. and Kool, E. C., Origins of the large differences in stability of DNA and RNA helixes: C-5 methyl and 2′-hydroxyl effects. *Biochemistry*, 1995, **34**, 4125–4132.
34. Šponer, J. *et al.*, The DNA and RNA sugar–phosphate backbone emerges as the key player. An overview of quantum-chemical, structural biology and simulation studies. *Phys. Chem. Chem. Phys.*, 2012, **14**, 15257–15277.
35. Pavelka, M. and Burda, J. V., Pt-bridges in various single-strand and double-helix DNA sequences. DFT and MP2 study of the cisplatin coordination with guanine, adenine, and cytosine. *J. Mol. Model.*, 2007, **13**, 367–379.
36. Sherrill, C. D., Computations of non-covalent π-interactions. In *Reviews in Computational Chemistry* (eds Lipkowitz, K. B. and Cundari, T. A.), John Wiley, New Jersey, 2009, vol. 26, pp. 1–38.
37. Tschumper, G. S., Reliable electronic structure computations for weak noncovalent interactions in clusters. In *Reviews in Computational Chemistry* (eds Lipkowitz, K. B. and Cundari, T. A.), John Wiley, New Jersey, 2009, vol. 26, pp. 39–90.
38. Grimme, S., Accurate description of van der Waals complexes by density functional theory including empirical corrections. *J. Comput. Chem.*, 2004, **25**, 1463–1473.
39. Grimme, S., Semiempirical hybrid density functional with perturbative second order correlation. *J. Chem. Phys.*, 2006, **124**, 034108.
40. Zhao, Y. and Truhlar, D. G., The M06 suite of density functionals for main group thermochemistry, thermochemical kinetics, noncovalent interactions, excited states, and transition elements: two new functionals and systematic testing of four M06-class functionals and 12 other functionals. *Theor. Chem. Acc.*, 2008, **120**, 215–241.
41. Grimme, S., Density functional theory with London dispersion corrections. *WIREs Comput. Mol. Sci.*, 2011, **1**, 211–228.
42. Grimme, S., Semiempirical GGA-type density functional constructed with a long-range dispersion correction. *J. Comput. Chem.*, 2006, **27**, 1787–1799.
43. Grimme, S., Antony, J., Ehrlich, S. and Krieg, H., A consistent and accurate *ab initio* parametrization of density functional dispersion correction (DFT-D) for the 94 elements H-Pu. *J. Chem. Phys.*, 2010, **132**, 154104.
44. dftd3 program; http://toc.uni-muenster.de/DFTD3/
45. Goerigk, L., Kruse, H. and Grimme, S., Benchmarking density functional methods against the S66 and S66x8 datasets for non-covalent interactions. *Chem. Phys. Chem.*, 2011, **12**, 3421–3433.
46. Shui, X., Sines, C. C., McFail-Isom, L., VanDerveer, D. and Williams, L. D., Structure of the potassium form of CGCGAATTCG-CG: DNA deformation by electrostatic collapse around inorganic cations. *Biochemistry*, 1998, **37**, 16877–16887.
47. Eichkorn, K., Treutler, O., Öhm, H., Häser, M. and Ahlrichs, R., Auxiliary basis sets to approximate Coulombic potentials. *Chem. Phys. Lett.*, 1995, **240**, 283–290.
48. Ahlrichs, R., Bär, M., Häser, M., Horn, H. and Kölmel, C., Electronic structure calculations on workstation computers: the program system turbomole. *Chem. Phys. Lett.*, 1989, **162**, 165–169.
49. Zheng, G., Lu, X.-J. and Olson, W. K., Web 3DNA – a web server for the analysis, reconstruction, and visualization of three-dimensional nucleic-acid structures. *Nucleic Acids Res.*, 2009, **37** (web server issue), W240-W246.
50. Biegler-König, F., Schönbohm, J., Derdau, R., Bayles, D. and Bader, R. F. W., AIM 2000, Version 1, Bielefeld, Germany, 2000.
51. Parthasarathi, R., Subramanian, V. and Sathyamurthy, N., Hydrogen bonding without borders: an atoms-in-molecules perspective. *J. Phys. Chem. A*, 2006, **110**, 3349–3351.

ACKNOWLEDGEMENTS. N.S. is an Honorary Professor at the Jawaharlal Nehru Centre for Advanced Scientific Research, Bengaluru. N.S. thanks the Department of Science and Technology, New Delhi for the J.C. Bose National Fellowship.

Received 19 June 2014; revised accepted 13 January 2015

In silico prediction of gene knockout candidates in *Escherichia coli* genome-scale model for enhanced succinic acid production from glycerol

Bashir Sajo Mienda[1,]*, Mohd Shahir Shamsir[1] and Rosli Md Illias[2]

[1]Bioinformatics Research Group, Biosciences and Health Sciences Department, Faculty of Biosciences and Medical Engineering, and [2]Department of Bioprocess Engineering, Faculty of Chemical Engineering, Universiti Teknologi Malaysia, 81310 Skudai, Johor, Malaysia

The use of genome-scale models of *Escherichia coli* to guide future metabolic engineering strategies for increased succinic acid production has received renewed attention in recent years. Substrate selectivity such as glycerol is of particular interest, because it is currently generated as a by-product of biodiesel industry and therefore can serve as a solitary carbon source. However, study on the prediction of gene knockout candidates for enhanced succinate production from glycerol using Minimization of Metabolic Adjustment Algorithm with the OptFlux software platform remained underexplored. Here, we show that metabolic engineering interventions by gene knockout simulation of some pyruvate dissimilating pathway enzymes (lactate dehydrogenase A and pyruvate formate lyase A) using *E. coli* genome-scale model can reduce acetate flux and enhance succinic acid production under anaerobic conditions. The introduced genetic perturbations led to substantial improvement in succinate flux of about 597% on glycerol and 120% on glucose than that of the wild-type control strain BSKO. We hypothesize that the deletion of pyruvate formate

*For correspondence. (e-mail: bsmienda@gmail.com)